SAKARYA ÜNİVERSİTESİ
FEN BİLİMLERİ ENSTİTÜSÜ DERGİSİ

Sakarya University Journal of Science
SAUJS

e-ISSN 2147-835X | Period Bimonthly | Founded: 1997 | Publisher Sakarya University |
http://www.saujs.sakarya.edu.tr/en/

Title: Structural and Microhardness Studies of Rare-Earth Doped Ruddlesden−Popper Manganites

Authors: Sevgi POLAT ALTİNTAS
Recieved: 2020-05-03 21:40:47

Accepted: 2020-11-18 21:38:03

Article Type: Research Article

Volume: 25
Issue: 1
Month: February
Year: 2021
Pages: 100-112

How to cite
Sevgi POLAT ALTİNTAS; (2021), Structural and Microhardness Studies of Rare-Earth Doped Ruddlesden−Popper Manganites. Sakarya University Journal of Science, 25(1), 100-112, DOI: https://doi.org/10.16984/saufenbilder.731354
Access link
http://www.saujs.sakarya.edu.tr/en/pub/issue/58068/731354

Sakarya University Journal of Science 25(1), 100-112, 2021

Structural and Microhardness Studies of Rare-Earth Doped Ruddlesden–Popper Manganites

Sevgi POLAT ALTİNTAS[1*]

Abstract

We investigate the explicit role of the A-site doping by Pr and Sm on the mechanical and structural features of the lanthanum based double-layered manganites. The polycrystalline samples of the Ruddlesden-Popper $(La_{1-y}RE_y)_{1.4}Ca_{1.6}Mn_2O_7$ phase with RE: Pr and Sm are elaborated by the solid-state synthesis route. Powder X-ray analysis reveal that the samples structure is tetragonal (I4/mmm space group) and the lattice parameters do not change significantly with the rare-earth substitution. However, the scanning electron microscopy analyses demonstrate that the substitution with Pr and Sm affects the microstructure, significantly. Vickers micro-hardness measurements are performed on both samples to evaluate several structural parameters such as the stiffness, creep, micro-hardness, etc. We compare and construct the mechanical and microstructural changes due to the Sm and Pr doping with La site. The detailed explanations for the observed mechanical changes by Pr and Sm doping is given.

Keywords: Ruddlesden-Popper phase, rare-earth substitution, microhardness, IIC and HK models

1. INTRODUCTION

Due to the potential applications in technology and exotic physical properties, perovskite manganites have been devoted much attention, recently. For instance, magnetic manganite materials have been used as the key ingredient for building some technological devices such as magnetic recording and readout equipment, highly sensitive magnetic-field sensors, solid oxide fuel cells, and refrigerators [1-3]. The general formula of the chemical compound given as $(RE, A)_{n+1}Mn_nO_{3n+1}$ is the well-known rare earth-doped perovskite manganite of the Ruddlesden–Popper series [4]. Here RE denotes a trivalent rare earth ion, while A represents the divalent alkaline earth ion, and n is the number of MnO_2 layers per unit cell. The simple perovskite manganites with $n = \infty$ have been deeply investigated which have a three-dimensional Mn-O networks and exhibit several novel physical phenomena [5-7]. The double layered manganite series with n=2, the MnO_2 sheets are isolated by

* Corresponding Author: sevgialtintas@ibu.edu.tr
[1]Abant İzzet Baysal University,,Bolu, Turkey, ORCID: https://orcid.org/0000-0002-3133-5693

two (RE, A)O planes which keeps the bilayer slices of MnO_6 octahedra. The reduced dimensionality and structural anisotropy introduce great effect on the physical properties of these manganites. The double layered manganite series have been found to exhibit an anisotropic reduction in the one-electron (e_g) bandwidth. The magnetic, electronic and structural features of the double layered manganite series are very interesting and apparently different from the those of exhibited by cubic perovskites [8-12]. In general, the mixed Mn^{3+}/Mn^{4+} valence state causes magneto-transport phenomena. One may expect interesting magneto-transport properties exhibited by the manganites in terms of anisotropic transport and exchange interactions [13,14].

Application of strong magnetic fields during magnetoresistance (MR) measurements is shown to induce large stresses in colossal magnetoresistance materials. Recent studies showed that determining the elastic moduli of the polycrystalline materials is crucial to reveal the binding forces and to understand thermodynamic features of the solid materials [15-20]. Beside the magnetic and the electric property investigations, exploration the elastic properties are also important to find the convenient material in the use of polycrystalline materials applications in technology.

Recent studies have been mainly focused on the transport, electrical and structural properties or the technological applicational area of the mixed valence manganites. On the other hand, there are few studies that investigates the elastic features of the layered manganites [15-17,21]. Specifically, a recent study [21] have been shown that the Nd and Gd rare earth doping with La site have prominent effects on the mechanical and structural features of $LaCaMnO_7$ compound. In this study [21], the apparent micro-hardness values of the Nd and Gd doped samples shows an enhancement with increasing the external load (an effect known as reverse indentation size effect which will be elaborated later in the text). In the present contribution, we investigate the role of Pr and Sm substitution with La on the mechanical and structural properties of the double layered manganites with chemical formula $(La_{1-y}RE_y)_{1.4}Ca_{1.6}Mn_2O_7$ (y: 0.857, 0.5). The explicit role of the external load force on the apparent micro-hardness values for the Pr and Sm doped compounds have been revealed. The true micro-hardness values under different external loads for the considered rare-earth substitution elements have also been investigated.

2. EXPERIMENTAL DETAILS

We used the standard solid-state reaction technique to prepare the polycrystalline bulk samples which are formulated as $(La_{0.142}Pr_{0.857})_{1.4}Ca_{1.6}Mn_2O_7$ (LPCMO) and $(La_{0.5}Sm_{0.5})_{1.4}Ca_{1.6}Mn_2O_7$ (LSCMO). In the formulation, the A-site average ionic radius is kept constant at $\langle r_A \rangle \approx 1.32$ Å. The average ionic radii for rare earth and calcium ions are computed according to Shannon's ionic radii with twelve-coordination number (La^{3+} (1.36 Å), Sm^{3+} (1.24 Å), Pr^{3+} (1.49 Å) and Ca^{2+} (1.34 Å)). The precursor powders were first heated 2 hours at 800 °C. The stoichiometric amounts of La_2O_3, Pr_2O_3, Sm_2O_3, $CaCO_3$ and Mn_2O_3 (Alfa Aesar, >99.9%) were thoroughly mixed for 4 hours with acetone to homogenize the mixture preliminary to the solid-state formation of manganite. Then they are calcined at 1150 °C for 24 hours with two intermediate grindings. The powders were consolidated into pellets of approximate dimensions 13 mm (diameter)×1.5 mm (thickness) by using a hydraulic press with an applied pressure of 3000 psi at room temperature. The final sintering was done at the temperature 1250 °C for 24 hours by slowly heating and cooling rate.

X-ray diffraction was used to carry out the structural characterization. The XRD instrument uses CuKα radiation at 1.5418 Å wavelength (Rikagu D/Max – IIIC diffractometer). The diffraction angle (2θ) was changed from 20º to 80º with 0.01° step size. The count time for each step was 1 s. Rietveld method in Jana2007 software package was used to analyze the experimental outputs [22]. Scanning electron microscope (Jeol 6390-LV) was used to investigate the role of the rare earth doping on the changes in the grain size, growth and morphology. 10 measurements (in

average) at random points were performed by the energy dispersive X-ray (EDX) spectrometer inside the scanning electron microscope in order to make a good prediction on the La, Pr, Sm, Ca and Mn contents. The indentation measurements were performed with a UMT–Bruker SYS2 coded mechanical tester which uses a Vickers type indenter. We aim to elucidate the effect of the applied loading force during the indentation. Therefore, an increasing loading force, such as (800, 1200, 1600, 2000) mN, was implemented during 10 seconds at room temperature (approximately 300 K).

3. RESULTS AND DISCUSSIONS

3.1. XRD and SEM Analysis

The powder XRD patterns for the polycrystalline $(La_{0.142}Pr_{0.857})_{1.4}Ca_{1.6}Mn_2O_7$ and $(La_{0.5}Sm_{0.5})_{1.4}Ca_{1.6}Mn_2O_7$ recorded at room temperature are demonstrated in Fig. 1. XRD data were analyzed using Rietveld refinement in Jana2006 program. Refinements were carried out in the $Sr_3Ti_2O_7$-type with a body-centered tetragonal unit cell (space group I4/mmm, JCPDS card no. 41–1488). Legendre polynomials consisting of 36 terms were used to model the background. Here the peak shape is identified by the pseudo-Voight function. Fig. 2 demonstrates the X-ray diffraction patterns which includes the fitted profile, the raw data as well as the difference profile for the rare earth doped samples. We observe an agreement between the observed and calculated intensities and positions of the lines which suggest that the considered samples have $Sr_3Ti_2O_7$-type perovskite structure [23]. We would like to remark here that a small amount of ABO3-type structure is found in X-ray pattern which can be considered as an additional phase in the multiphase refinement (see the phase 2 in Fig. 2). Table 1 summarizes the relevant structural parameters and the quality factors obtained from Rietveld analysis.

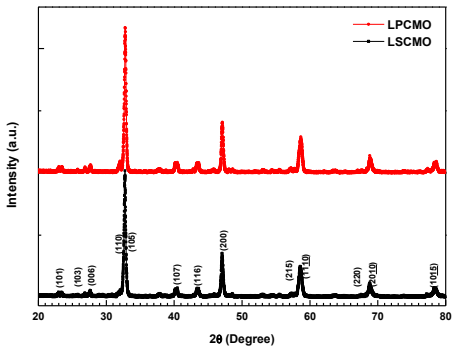

Figure 1 Powder X-ray diffraction pattern of the LPCMO and LSCMO samples.

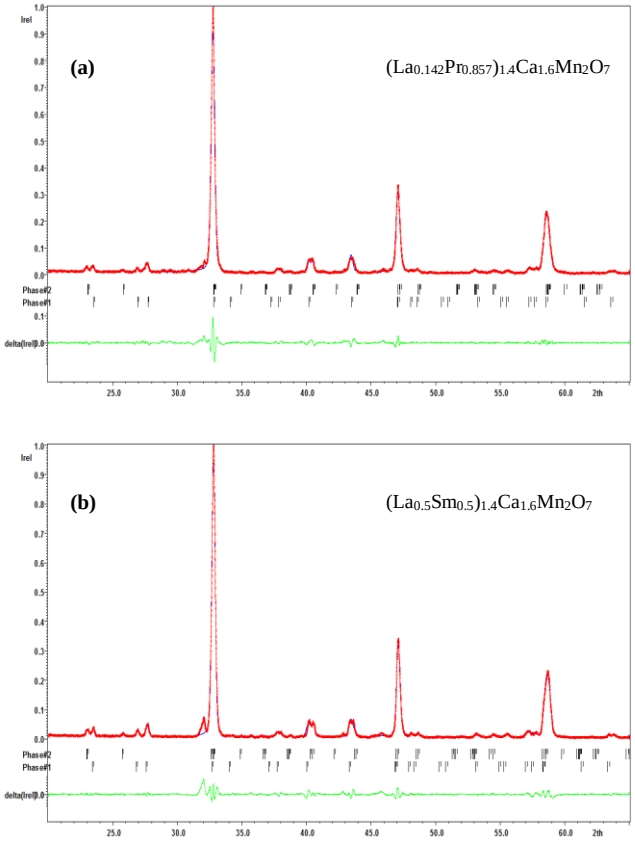

Figure 2. (Color online.) Rietveld profiles considering I4/mmm space group for the samples (a) LPCMO and (b) LSCMO. Here the red line corresponds to the observed XRD pattern, while blue line indicates the calculated XRD pattern. The black vertical bars represent the Bragg positions, and the green line (at the bottom) shows the difference between the calculated and the observed XRD diagram.

Table 1
Refined structural parameters, unit cell volume, R-factors and average crystallite size of bilayered manganites.

Structure		
T e t r a g o n a l e		
Space Group I4 / m m m		
$\langle r_A \rangle$ = ***1.3213*** Å		
	LPCMO	LSCMO
a(Å)	3.869816	3.857851
Δa	0.000509	0.000347
c(Å)	19.38771	19.29455
Δc	0.00287	0.00166
V(Å^3)	290.3403	287.1611
ΔV	0.0687	0.0338
GOF	1.44	1.14
R_p	9.53	9.21
R_{wp}	15.65	12.89
<D>(nm)	61	53

We calculate the average crystallite size by using the Scherrer formula through measuring the full width at half maximum of the diffraction line in the XRD patterns. The Scherrer formula is given by $D = k\lambda/\beta \cos\theta$. Here D is the measure of the average crystallite size, k is the shape factor (which is 0.89), λ= 1.5418 Å is the wavelength of X-ray source, θ is the diffraction angle for the highest intense peak (with Miller index (106) on the Bragg angle 2θ=32.79°) and β is the full-width at half maximum of each diffraction peak in the radian unit [24, 25]. The refinement values are tabulated in Table 1.

The SEM micro-graphs shown in Fig.3 explicitly demonstrate that the surface morphology and the grain size are uniform, homogenous and also dense for the Pr and Sm doped samples. The measurements of the average grain sizes of the samples were performed from several SEM micrographs by using the ImageJ software. Based on Gaussian fitting method, average grain size is obtained to be 1.61 μm for LPCMO and 1.43 μm for LSCMO samples. The energy dispersive analysis of EDX spectrums of both samples are presented in the below of the SEM pictures in Fig. 3. The elemental concentrations of the considered samples are checked by using EDX analysis and no impurity peaks are observed.

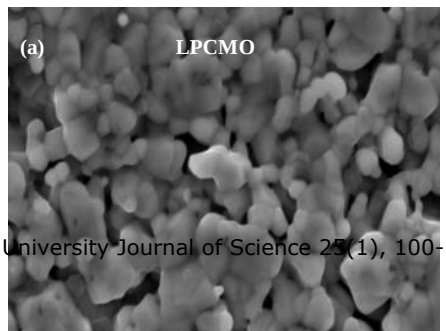

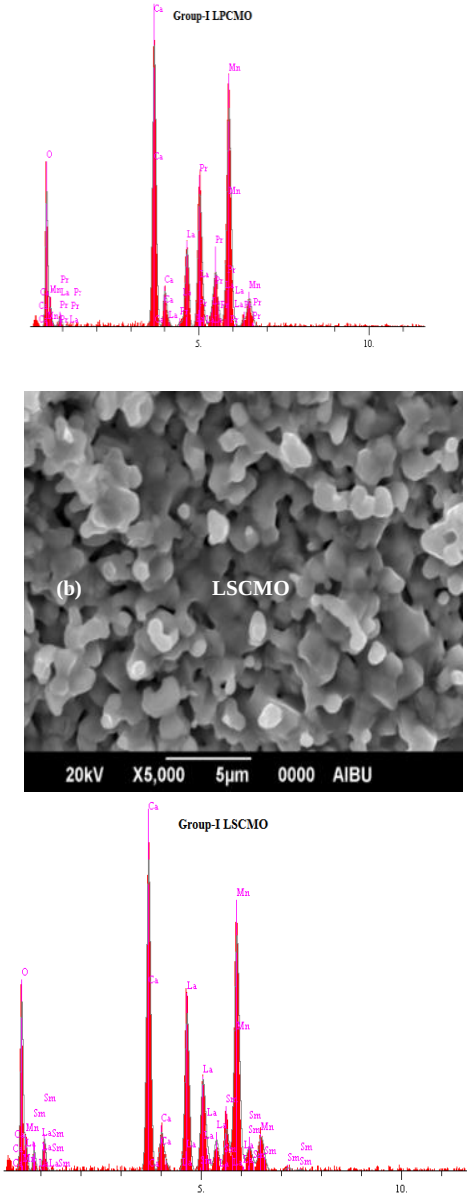

Figure 3 SEM micrographs for **(a)** LPCMO and **(b)** LSCMO bilayered manganites revealing surface morphologies.

3.2. Dynamic micro-hardness measurements

The aim of the present contribution is to investigate the changes in the mechanical properties of LPCMO and LSCMO composite samples via the Pr and Sm substitution. Along this aim, we measure the load dependent contact length. Using the Vickers hardness tester, micro-hardness measurements are performed for the applied loads between 400 mN and 2000 mN values. The dynamic indentation measurements

give the loading and unloading penetration depth relation [26, 27]. It is well known that during the loading and unloading stages, the materials are subject to a process where plastic and elastic deformations occur. In a similar way, we expose our samples to elastic and plastic deformation processes during the loading and unloading stages. The mechanical properties of the samples are calculated by using techniques introduced by the Oliver and Pharr in Ref. [28].

Figs. 4 and 5 show the applied load and unload forces as a function of the contact depth for LPCMO and LSCMO samples, respectively. In addition, we present a contact depth, hc, extracted from the unloading curve for Pr substituted sample in the inset of Fig. 4. The same method is used to evaluate the value of hc for the LSCMO sample for each load and tabulated in Table 2. We calculate the values of hc for the LPCMO sample as 8.8992 μm and 22.469 μm at applied unloading force 400 mN and 2000 mN, respectively. Morover, the similar values for LSCMO sample are 10.9221 μm and 17.9106 μm at the unloading force 400 mN and 2000 mN, respectively. The variation in the hc for the LPCMO sample is obviously greater than that of the LSCMO sample. This result indicates that the Pr substituted sample has more plastic deformation and less elastic recovery than that of the Sm substituted sample.

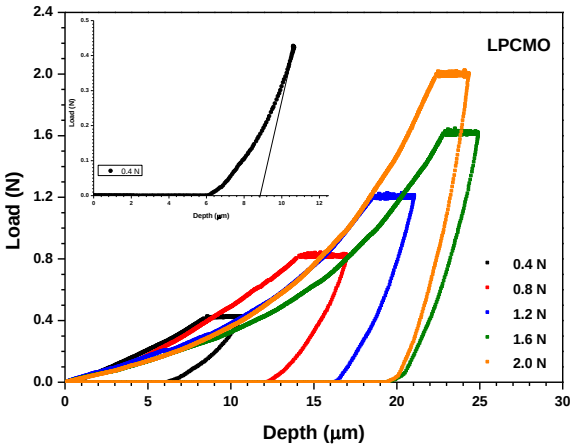

Figure 4 Loading/unloading versus depth curve for the LPCMO sample. Inset shows the contact depth, h_c, extracted from the unloading curve.

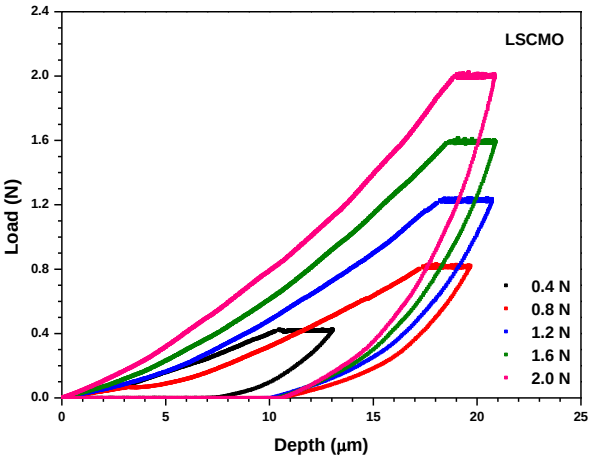

Figure 5 Loading/unloading versus depth curve for the LSCMO sample.

Now we investigate the area of the indent imprint which describes the cross-sectional area of the indenter in a given distance at the back of its tip. The area can be calculated as [28],

$$A_c = \pi h_c^2 \tan^2\alpha \qquad (1)$$

where α is 70.3° for a Vickers or Berkovich indenter. Therefore, the area A_c is given as $24.5h_c^2$. The A_c values are calculated by using Eq. (1) for the Pr and Sm substituted samples and are tabulated in Table 2. It is seen here that the A_c values for the both samples are monotous with the applied loads. In other words, A_c decreases with the decreasing loads.

Table 2

h_c, h_{max}, A_c, Creep, S, H and E_r values as a function of applied load for the samples LSCMO and LPCMO. All parameters are defined in the text.

Sample	P_{max} *(N)*	h_c *(μm)*	h_{max} *(μm)*	A_c *(m^2)*	*Creep (μm)*	*S (MN/m)*	*H (G Pa)*	E_r *(GPa/m)*
LPCMO	0.4	8.89	10.64	1.93E-09	1.97	0.229	0.206	4.619
LPCMO	0.8	15.07	17.00	5.56E-09	2.89	0.413	0.144	4.913
LPCMO	1.2	19.0	21.04	8.84E-09	2.53	0.589	0.136	5.549
LPCMO	1.6	22.68	24.9	1.26E-08	2.15	0.723	0.127	5.706
LPCMO	2.0	22.46	24.33	1.23E-08	1.89	1.074	0.162	8.561
LSCMO	0.4	10.92	12.98	2.92E-09	2.54	0.193	0.136	3.174
LSCMO	0.8	16.97	19.62	7.06E-09	2.22	0.303	0.113	3.192
LSCMO	1.2	17.49	20.72	7.50E-09	2.48	0.372	0.159	3.807
LSCMO	1.6	17.69	20.89	7.67E-09	2.25	0.500	0.208	5.063
LSCMO	2.0	17.91	20.86	7.85E-09	1.94	0.678	0.254	6.776

Creep (also called cold flow) of a solid material is a proper quantity to indicate its response under persistent mechanical stress. Therefore, the creep behavior of the two samples at all loads are computed and tabulated in Table 2. The creep within material can exist under indentation loading and reveals itself as a change of the indentation depth with a fixed applied loading force [29]. It is interesting to note that while the creep of a Pr doped sample has a non-monotonous behavior, the Sm doped one has a linear response to the applied load. When we compare the creep values for the two doped samples, we observe that the Sm doped results, in general, higher creep values than the Pr doped one. The two samples encounter the same loading process and experimental conditions. The differences in the creep values as given in Table 2 is, therefore,

caused by the different doped sample with La side.

The sudden displacement discontinuity in the indentation loading and unloading curves evidences the effect of pop-in and pop-out in the materials, respectively [30]. However, the pop-in and pop-out behaviors for the LPCMO and the LSCMO samples are not obtained at any applied loads in our experiment. Therefore, we conclude that Sm or Pr substitution with La-site significantly effects the crystal structure in a way which prevents the sudden mechanical discontinuities in the indentation processes.

We have also calculated the micro-indentation hardness by using the following formula [31]:

$$H = \frac{P_{\max}}{A_c} = \frac{P_{\max}}{24.5 * h_c^2} \quad (2)$$

where P_{max} is the maximum value of the applied load force for each cycle and A_c is the contact area values as defined in Eq. (1). Using P_{max} values in Figs. 4 and 5, the hardness values are plotted in Fig. 6 as a function of applied loads and the numerical values are tabulated in Table 2. It is clear that the apparent hardness values significantly affected by the applied loads as well as the nature of the rare-earth element. As can be seen from Fig. 6 that the hardness values of LPCMO sample decrease with the increase in load. On the contrary, the H values for LSCMO sample increases linearly with load. The linear increase of the hardness values as a function of load is the indication of reverse indentation size effect (RISE) for Sm doped sample [32, 33]. On the other hand, the decrease of H values with the increase in applied loads shows the presence of indentation size effect (ISE) in the Pr doped sample [34]. It is recently shown that plastic, elastic and mixed plastic-elastic deformation response of the material under external loads are the prominent mechanisms that might cause ISE [35-38]. More specifically, the dislocation loops formed by indentation [35, 36] and dislocations due to strain gradients [37] are the examples of such mechanisms that result in ISE. Moreover, the indenter or specimen friction resistance interacting with the elastic resistance of a material are another source example of the ISE [38]. On the other hand, the effect of distortion zones [39], bluntness of the indenter and clipping of the specimen around the indentation region [40] are some example mechanisms that might cause RISE behavior. We would like to mention here that a recent study [21] investigated the explicit role of the Nd and Gd doping with La site on the mechanical and structural features of $LaCaMnO_7$ compound. In this study, the apparent micro-hardness values of the considered compounds enhance with the applied load. In other words, the Nd and Gd substitution results in RISE. Our results demonstrate that the Pr doped sample, on the contrary, results in ISE.

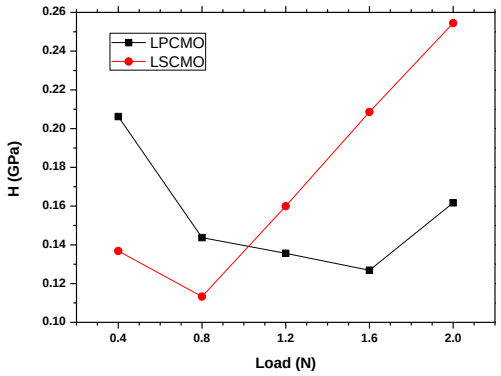

Figure 6 The apparent hardness values as a function of load for the samples LPCMO and LSCMO.

The true hardness values for our considered compounds are evaluated by using the experimental data. The methods known as indentation induced cracking (IIC) and the Hays-Kendall (HK) are appropriate to evaluate the true hardness values for the samples that exhibits RISE and ISE behaviors, respectively [39, 41]. The LSCMO sample exhibits RISE behavior as noted above. Therefore, we fit the experimental data to IIC model which is given as:

$$H_{IIC} = K(P^{5/3}/h_c^3)^m \quad (3)$$

Here m and K values are constants and independent of the type of the material and the load. In Fig. 7, we plot Ln(H) versus Ln($P^{5/3}/h_c^3$) graph for the Sm doped sample. The slope gives

the extracted m values which is calculated as 0.56 for the LSCMO sample. It explicitly proves that doping with Sm results in RISE behavior. The vertical intercept in the figure gives the true hardness value of the LSCMO sample which is approximately 2.82 GPa. We would like to mention here that the applied load (2N) shown in Fig.6 is not sufficient to approach the plateau region.

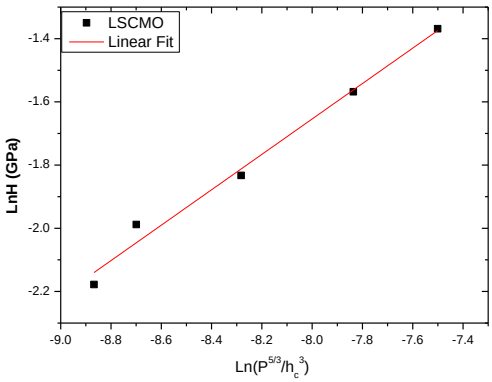

Figure 7 *Ln(H)* versus $Ln(P^{5/3}/h_c^3)$ graph for the LSCMO sample. The fitted line is obtained by using the IIC model as defined in the text.

For the LPCMO sample, we use the HK model to show the ISE behavior which is given as:

$$P\text{-}P_{0HK} = K_1 h_c^2 \qquad (4)$$

Here P_{0HK} is the value of the minimum applied load and K_1 is the hardness constant which is independent of the applied load. It is obvious from the equation that the effective indentation load ($P\text{-}P_{0HK}$) is directly related to the square of the indentation diagonal length. In the considered model, true hardness, H_{HK}, is calculated as

$$H_{HK} = 1854.4K_1 \ \text{(GPa)} \qquad (5)$$

Fig. 8 shows the applied load F as a function of d^2 with the aim to examine the data using the HK model. Here we obtain a linear dependence of F on d^2 for the Pr substitution. H_{HK} and linear regression coefficent (LRC) fit parameters are calculated as 0.125 GPa and 0.9994, respectively. As can be seen from Fig. 6 that while the apparent hardness value of LPCMO sample reaches almost the plateau region, the true hardness value is indeed in the plateau region.

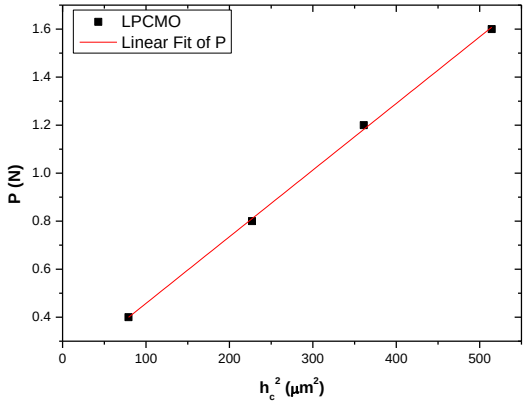

Figure 8 Load versus the squared of contact depth for the LPCMO sample. The fitted line is obtained by using the HK model.

There are several successful methods to calculate the stiffness of a sample [42-46]. A direct way to calculate the stiffness is to make a linear fit to the fraction of the highest portion of the unloading curve. The slope of the fitted line gives the stiffness of the specimen for a single load. The stiffness (S) is computed as [43]:

$$S = \left|\frac{dP}{dh}\right| = \frac{\sqrt{2}}{\pi}\cdot\frac{E_r}{\sqrt{A_c}} \qquad (6)$$

Here E_r indicates the reduced elastic modulus. The S values are tabulated in Table 2. One can note from the table that the S values depends on the load significantly. The increase in the load increases the S values for both samples. When we analyze the dopant effects, we observe that Pr doping results in higher S values than the Sr doped sample at all loads. The reduced elastic modules as a function of load can be evaluated by using the Eq. (6) and are displayed in Table 2 and Fig. 9. It is observed that the values for the considered rare-earth samples increase as a function of load.

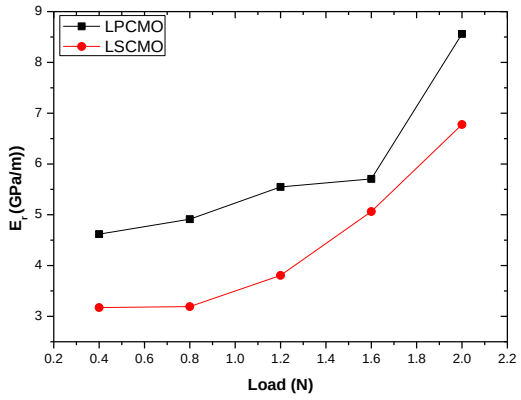

Figure 9 The elastic modulus as a function of applied load for the samples LPCMO and LSCMO.

We can calculate the percentage elastic recovery ratio (%), ERR, using the load and unload curves.

$$ERR = \frac{h_{max} - h_{min}}{h_{max}}.100 \qquad (7)$$

The ERR provides us to quantitatively compare the elastic features of the samples. One can calculate the ERR as in Eq. 7 where h_{max} (h_{min}) values indicate the maximum (non-recovery) contact depth in the indentation stage. In Fig.10, the ERR values of the samples are shown. We observe that while the ERR values of the LPCMO are in the range 20-50%, the ERR values for LSCMO sample recover more range approximately 40-50%. This shows that the ERR values for the LSCMO sample recovers better to its original shape than that of the LPCMO one at all the considered loads. Please remark here that both samples possess the same ionic A site radius ($<r_A> \approx 1.32$ Å). However, we found here that the considered samples have different responses to the plastic deformation. Even the ionic radius of the samples is the same, the mechanical properties, such as the elastic modulus, hardness and stiffness, are quite different. The differences are due to the different microstructures and average grain sizes. From the comparison of Sm or Pr doping effects, we conclude that Sm doping leads to denser surface, better grain connectivity and smaller average grain size. Moreover, Sm doped sample has the density of voids lower than the Pr doped one. We conclude here that the Sm doped sample has higher hardness values.

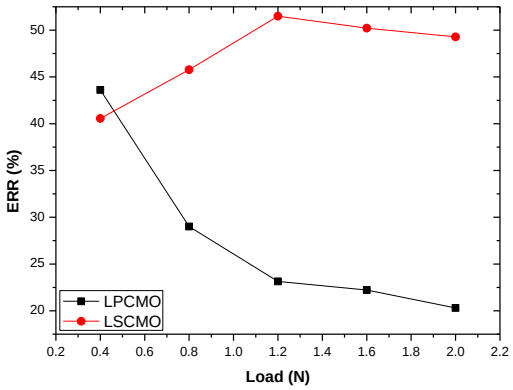

Figure 10 ERR values for LPCMO and LSCMO obtained at different loads.

4. CONCLUSIONS

We have given a comprehensive analysis on the mechanical and microstructural properties of the Ruddlesden-Popper $(La_{1-y}RE_y)_{1.4}Ca_{1.6}Mn_2O_7$ phase with RE: Pr and Sm. The explicit role of the Pr and Sm doping with La site has been revealed. The X-ray diffraction measurements demonstrate that all samples exhibit $Sr_3Ti_2O_7$-type perovskite structure with the I4/mmm space group. From the SEM micro-graphs analysis, it is found that the surface morphology and the grain size are uniform, homogenous and also dense for both samples. The dynamic Vicker micro-hardness measurements have been performed in order to study the mechanical properties. We have used the HK model for the LPCMO sample and the IIC model for the LSCMO to compute the true-hardness values. Our main conclusions can be listed as follows. The stiffness values of both samples depend on the load significantly which can increase as a function of the load. The both pop-in and pop-out behaviors for the samples are not observed at the considered loads. This is the indication that Pr and Sm doping have significance on the mechanical discontinuities. While the hardness value of the LPCMO sample decreases from 0.21 to 0.16 GPa for the load increasing from 400 to 2000 mN, the hardness value of the LSCMO sample increases from 0.14 to 0.25 GPa in the same load range. A RISE

behavior is observed for the LSCMO sample, in contrast to the LPCMO sample which exhibits ISE behavior. The true micro-hardness values of the LSCMO sample (which is 2.82 GPa) is considerably larger than that of the LPCMO (which is 0.125 GPa). The large deviation in the true micro-hardness values in the considered samples is due to the different average grain sizes and microstructures. The reduced elastic modules of the samples have been found to increase as the function of the load. The percentage elastic recovery ratio of the samples has opposite dependences on the load. While ERR values of the LSCMO sample increase as a function of the load, the values of the LPCMO decrease.

Acknowledgments

The author gratefully acknowledges support by Bolu Abant Izzet Baysal University, Scientific Research Projects Program under the Grant 2017.03.02.1238.

Funding

The author has no received any financial support for the research, authorship or publication of this study.

The Declaration of Conflict of Interest/ Common Interest

No conflict of interest or common interest has been declared by the author.

The Declaration of Ethics Committee Approval

This study does not require ethics committee permission or any special permission.

The Declaration of Research and Publication Ethics

The author of the paper declare that they comply with the scientific, ethical and quotation rules of SAUJS in all processes of the paper and that they do not make any falsification on the data collected. In addition, they declare that Sakarya University Journal of Science and its editorial board have no responsibility for any ethical violations that may be encountered, and that this study has not been evaluated in any academic publication environment other than Sakarya University Journal of Science.

REFERENCES

[1] F. Ben Jemaa, S. Mahmood, M. Ellouze, E.K. Hlil, F. Halouani, I. Bsoul, M. Awawdeh, "Structural, magnetic and magnetocaloric properties of $La_{0.67}Ba_{0.22}Sr_{0.11}Mn_{1-x}Fe_xO_3$ nanopowders", Solid State Sciences, vol. 37, pp. 121-130, 2014.

[2] P. Ripka and M. Janosek, "Advantages in magnetic field sensors," IEEE Sensors Journal, vol. **10**, no. 6, pp. 1108–1116, 2010.

[3] M. A. Mamun, A. Haque, A. Pelton, B. Paul and K. Ghosh, "Structural, electronic, and magnetic analysis and device characterization of ferroelectric-ferromagnetic heterostructure (BZT-BCT/LSMO/LAO)," IEEE Transactions on Magnetics., vol. 54, no. 12, pp. 1-8, 2018.

[4] S. N. Ruddlesden and P. Popper, "New compounds of the K_2NiF_4 type," Acta. Crystallographica, vol. 10, pp. 538-539, 1957.

[5] L. L. Lev, J. Krempaský, U. Staub, V. A. Rogalev, T. Schmitt, M. Shi, P. Blaha, A. S. Mishchenko, A. A. Veligzhanin, Y. V. Zubavichus, M. B. Tsetlin, H. Volfová, J. Braun, J. Minár, and V. N. Strocov, "Fermi Surface of Three-Dimensional $La_{1-x}Sr_xMnO_3$ Explored by Soft-X-Ray ARPES: Rhombohedral Lattice Distortion and Its Effect on Magnetoresistance," Physical Review Letters, vol. 114, no. 23, pp. 237601, 2015.

[6] R. Chourasia and O. P. Shrivastava, "Crystal structure and impedance study of samarium substituted perovskite: $La_{1-x}Sm_xMnO_3$ (x = 0.1–0.3)," Solid State Sciences, vol. 14, no. 3, pp. 341-348, 2012.

[7] S. Mori, C. H. Chen, and S.-W. Cheong, "Pairing of charge-ordered stripes in

(La,Ca)MnO_3", Nature, vol. 392, pp. 473-476, 1998.

[8] J.-S. Lee, C.-C. Kao, C. S. Nelson, H. Jang, K.-T. Ko, S. B. Kim, Y. J. Choi, S.-W. Cheong, S. Smadici, P. Abbamonte, and J.-H. Park "Fragile Magnetic Ground State in Half-Doped $LaSr_2Mn_2O_7$," Physical Review Letters, vol. 107, no. 3, pp. 037206, 2011.

[9] J.F. Mitchell, C.D. Ling, J.E. Millburn, D.N. Argyriou, A. Berger, M. Medarde, "Magnetic phase diagram of layered manganites in the highly doped regime," Journal of Applied Physics, vol. 89, no. 11, pp. 6618-6620, 2001.

[10] J. Q. Li, Y. Matsui, T. Kimura, and Y. Tokura, "Structural properties and charge-ordering transition in $LaSr_2Mn_2O_7$," Physical Review B, vol. **57**, no. 6, R3205-R3208, 1998.

[11] P. D. Battle, D. E. Cox, M. A. Green, J. E. Millburn, L. E. Spring, P. G. Radaelli, M. J. Rosseinsky, and J. F. Vente, "Antiferromagnetism, Ferromagnetism, and Phase Separation in the GMR System $Sr_{2-x}La_{1+x}Mn_2O_7$," Chemistry of Materials, vol. *9, no. 4*, pp. 1042-1049, **1997.**

[12] L. Vasiliu-Doloc, S. Rosenkranz, R. Osborn, S. K. Sinha, J. W. Lynn, J. Mesot, O. H. Seeck, G. Preosti, A. J. Fedro, and J. F. Mitchell, **"**Charge Melting and Polaron Collapse in $La_{1.2}Sr_{1.8}Mn_2O_7$," Physical Review Letters, vol. 83, no. 21, pp. 4393, 1999.

[13] M. Oumezzine, J. S. Amaral, F. J. Mompean, M. G. Hernandez, M. Oumezzine, "Structural, magnetic, magneto-transport properties and Bean-Rodbell model simulation of disorder effects in Cr^{3+} substituted $La_{0.67}Ba_{0.33}MnO_3$ nanocrystalline synthesized by modified Pechini method," RSC Advances, vol. 6, pp. 32193–32201, 2016.

[14] S. K. Mandal, T. K. Nath, and V. V. Rao, "Effect of nanometric grain size on electronic-transport, magneto-transport and magnetic properties of $La_{0.7}Ba_{0.3}MnO_3$ nanoparticles," J. Phys.: Condens. Matter, vol. 20, pp. 385203, 2008.

[15] Y. S. Reddy, V. P. Kumar, E. Nagabhushanam, P. Kistaiah, and C. V. Reddy, "Electrical, magnetic and elastic properties of $La_{1.2}(Sr_{1-x}Ca_x)_{1.8}Mn_2O_7$ ($0.0 \leq x \leq 0.4$)," Journal of Alloys and Compounds, vol. 440, no. 1–2, pp. 6–12, 2007.

[16] Y. S. Reddy, M. V. Ramana Reddy, P. Veerasomaiah, C. Vishnuvardhan Reddy, "Elastic properties of double layered manganite $La_{1.2}Sr_{1.8-x}Ca_xMn_2O_7$ (x=0–0.4)," Material Science (Poland), vol, 25, no. 3, pp. 619–626, 2007.

[17] Y. S. Reddy, P. Kistaiah, C. Vishnuvardhan Reddy, "Elastic properties of double layered manganites $R_{1.2}Sr_{1.8}Mn_2O_7$ (R = La, Pr, Nd, Sm)," Rare Metals, vol. 33, no. 2, pp. 166–170, 2014.

[18] G. Lalitha and P. Venugopal Reddy, "Elastic behavior of neodymium based manganites," Ultrasonics, vol. 52, pp. 706-711, 2012.

[19] C. Thiele, K. Dörr, O. Bilani, J. Rödel, and L. Schultz, "Influence of strain on the magnetization and magnetoelectric effect in $La_{0.7}A_{0.3}MnO_3$ / PMN−PT (001) (A = Sr , Ca)," Phys. Rev. B, vol. 75, no. 5, pp. 054408, 2007.

[20] J. J. U. Buch, G. Lalitha, T. K. Pathak, N. H. Vasoya, V. K. Lakhani, P. V. Reddy, Ravi Kumar and K. B. Modi, "Structural and elastic properties of Ca-substituted $LaMnO_3$ at 300 K," J. Phys. D: Appl. Phys., vol. 41, no. 2, pp. 025406, 2008.

[21] R. Terzioglu, "The structural and mechanical properties of Gd and Nd substituted double layered $LaCaMnO_7$ ceramics," Journal of Alloys and Compounds, vol. 797, pp. 1173–1180, 2019.

[22] V. Petříček, M. Dušek, and L. Palatinus, "Crystallographic Computing System JANA2006: General features," Zeitschrift für Kristallographie - Crystalline Materials, vol. 229, no. 5, 2014.

[23] JCPDS-International Centre for Diffraction Data Task Group on Cell Parameter Refinement," Powder Diffr., vol. 1, no. 1, pp. 66–76, 1986.

[24] De Keiyser, T. H., Langford, J. I., Mittemeijer, and Vogels, A. B. P., "Use of the Voigt function in a single-line method for the analysis of X-ray diffraction line broadening," J. Appl. Cryst., vol. 15, pp. 308- 314, 1982.

[25] P. E. Tomaszewski, "The uncertainty in the grain size calculation from X-ray diffraction data," Phase Transitions, vol. 86, no. 2–3, pp. 260–266, 2013.

[26] O. D. Neikov, Handbook of powders of non-ferrous metals. Oxford, UK; New York, NY: Elsevier, 2005.

[27] K. Higashitani, H. Makino, and S. Matsusaka, Powder Technology Handbook, 4th ed. Fourth edition. | Boca Raton, FL: Taylor & Francis Group, LLC, 2020.: CRC Press, 2019.

[28] W. C. Oliver and G. M. Pharr, "Measurement of hardness and elastic modulus by instrumented indentation: Advances in understanding and refinements to methodology," J. Mater. Res., vol. 19, no. 1, pp. 3–20, 2004.

[29] P. S. Phani and W. C. Oliver, "A direct comparison of high temperature nanoindentation creep and uniaxial creep measurements for commercial purity aluminum," Acta Materialia, vol. 111, pp. 31–38, 2016.

[30] J. E. Bradby et al., "Indentation-induced damage in GaN epilayers," Appl. Phys. Lett., vol. 80, no. 3, pp. 383–385, 2002.

[31] W. C. Oliver and G. M. Pharr, "Measurement of hardness and elastic modulus by instrumented indentation: Advances in understanding and refinements to methodology," J. Mater. Res., vol. 19, no. 1, pp. 3–20, 2004

[32] K. Sangwal, "On the reverse indentation size effect and microhardness measurement of solids," Materials Chemistry and Physics, vol. 63, no. 2, pp. 145–152, 2000.

[33] P. Feltham and R. Banerjee, "Theory and application of microindentation in studies of glide and cracking in single crystals of elemental and compound semiconductors," J Mater Sci, vol. 27, no. 6, pp. 1626–1632, 1992.

[34] W. D. Nix and H. Gao, "Indentation size effects in crystalline materials: A law for strain gradient plasticity," Journal of the Mechanics and Physics of Solids, vol. 46, no. 3, pp. 411-425, 1998.

[35] G.P. Upit, S.A. Varchenya, "Microhardness of alkali halide crystals," Physica Status Solidi B, vol. 17, no. 2, pp. 831–835, 1966.

[36] ed.) Westbrook J. H. (Jack Hall), ed.) Conrad Hans, and A. S. for Metals, "The Science of Hardness Testing and its Research Applications," ASME, Metals Park, Ohio: American Society for Metals, 1973.

[37] Q. Ma and D. R. Clarke, "Size dependent hardness of silver single crystals," J. Mater. Res., vol. 10, no. 4, pp. 853–863, 1995.

[38] H. Li and R. C. Bradt, "The microhardness indentation load/size effect in rutile and cassiterite single crystals," Journal of Materials Science, vol. 28, no. 4, pp. 917–926, 1993.

[39] K. Sangwal, "Microhardness of as-grown and annealed lead sulphide crystals," J Mater Sci, vol. 24, no. 3, pp. 1128–1132, 1989.

[40] P P. Feltham and R. Banerjee, "Theory and application of microindentation in studies of glide and cracking in single crystals of elemental and compound semiconductors," J Mater Sci, vol. 27, no. 6, pp. 1626–1632, 1992.

[41] M.L. Tarkanian, J.P. Neumann, L. Raymond, Determination of the temperature dependence of {1 0 0} and {1 1 2} slip in tungsten from Knoop hardness measurements, in: J.H. Westbrook, H. Conrad (Eds.), The Science of Hardness Testing and Its Research Applications, American Society for Metals, Metal Park, OH, pp. 187–198, 1973.

[42] J. Hay, P. Agee, and E. Herbert, "Continuous Stiffness Measurement During Instrumented

Indentation Testing," Experimental Techniques, vol. 34, no. 3, pp. 86–94, Jan. 2010.

[43] K. Zeng and C.-h Chiu, "An analysis of load–penetration curves from instrumented indentation," Acta Materialia, vol. 49, no. 17, pp. 3539–3551, 2001.

[44] W. C. Oliver and G. M. Pharr, "An improved technique for determining hardness and elastic modulus using load and displacement sensing indentation experiments," J. Mater. Res., vol. 7, no. 6, pp. 1564–1583, 1992.

[45] L. Arda, O. Ozturk, E. Asikuzun, and S. Ataoglu, "Structural and mechanical properties of transition metals doped ZnMgO nanoparticles," Powder Technology, vol. 235, pp. 479–484, 2013.

[46] M. B. Turkoz, Y. Zalaoglu, T. Turgay, O. Ozturk, B. Akkurt, and G. Yildirim, "Evaluation of key mechanical design properties and mechanical characteristic features of advanced Bi-2212 ceramic materials with homovalent Bi/Ga partial replacement: Combination of experimental and theoretical approaches," Ceramics International, vol. 45, no. 17, pp. 21183–21192, 2019.